Web Chapter 1

Image Gallery: General concepts of low dose CT

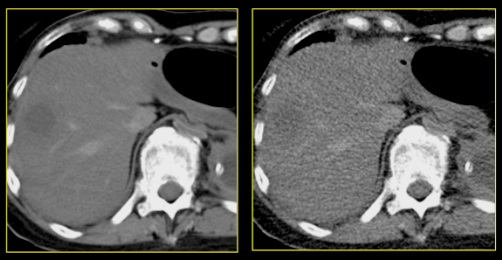

Sarabjeet Singh, MD
Mannudeep K. Kalra, MD
**James R. Stone, MD*
**Eugene J. Mark, MD*
James H. Thrall, MD

*Department of Radiology and *Department of Pathology*
Massachusetts General Hospital
Harvard Medical School, Boston

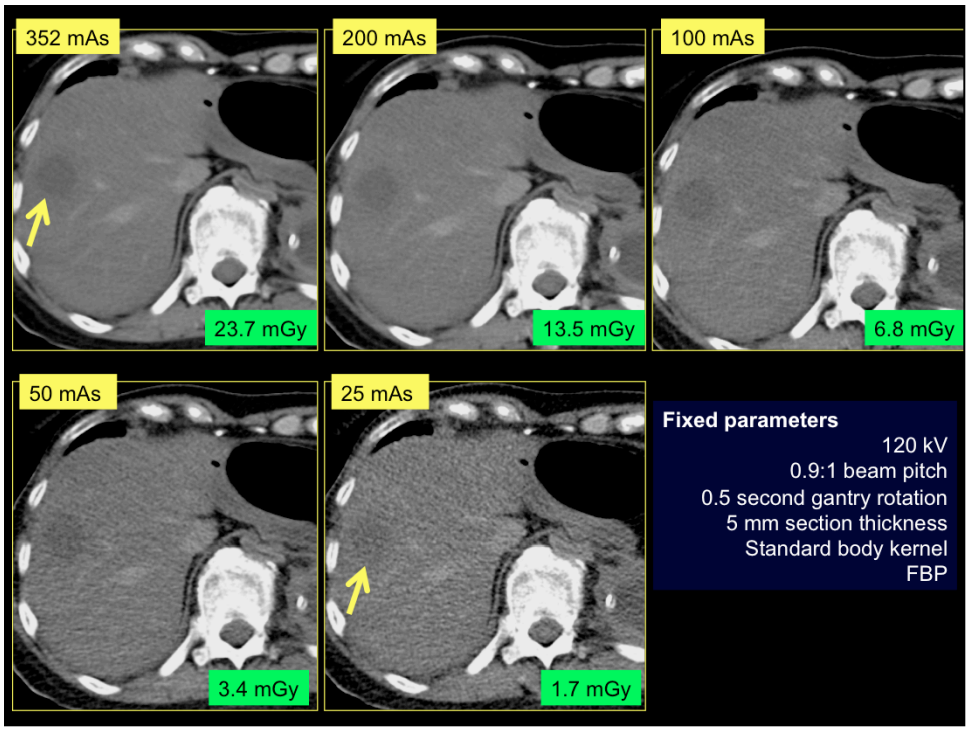

Figure 1a: 60 year old female (52 kg) with known diagnosis of metastatic papillary carcinoma of thyroid with post mortem abdominal CT at various tube current levels. Lower mAs images have higher image noise and lowered visibility of low attenuation hepatic metastases (arrow) and hepatic vessels.

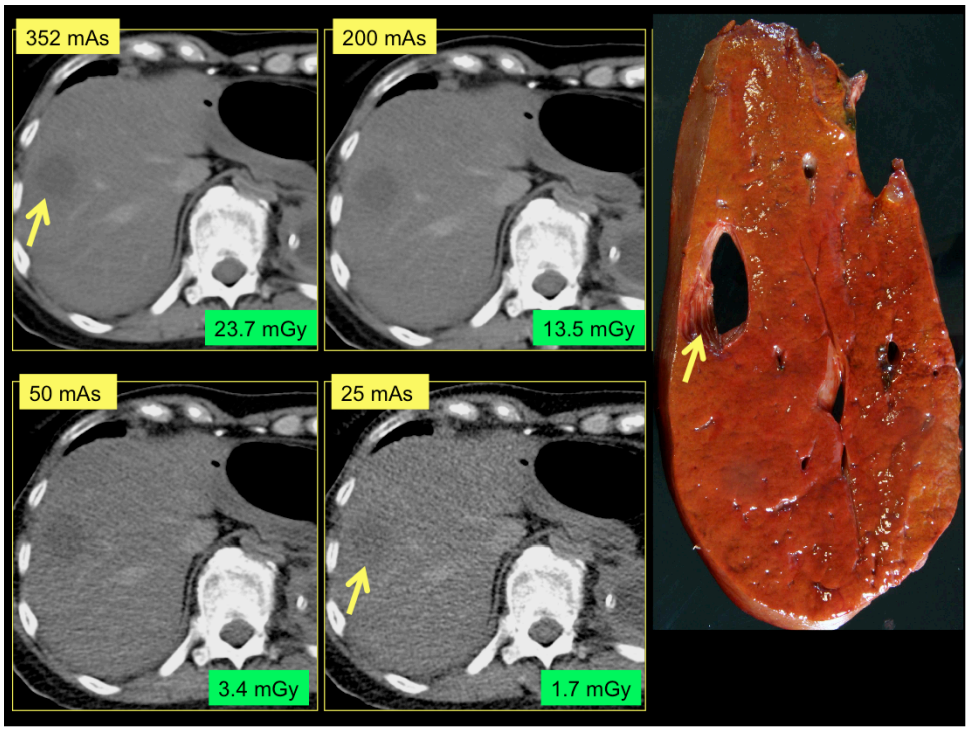

Figure 1b: 60 year old female (52 kg) with known diagnosis of metastatic papillary carcinoma of thyroid with post mortem abdominal CT at various tube current levels. Lower mAs images have higher image noise and lowered visibility of low attenuation hepatic metastases (arrow) and hepatic vessels.

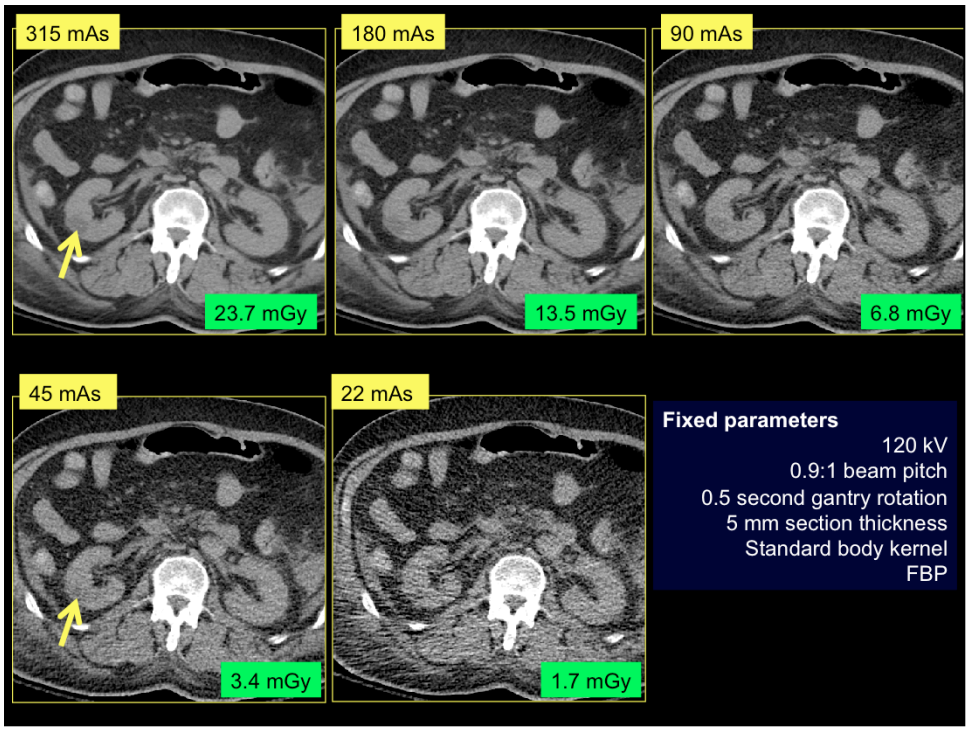

Figure 2a: Post mortem abdominal CT images of a 60 year old male (82 kg) at various tube currents. Image noise increases as the tube current is lowered and interferes with the visibility of right renal low attenuation lesion (arrow). His autopsy report confirmed presence of cysts in the mid and lower pole of the right kidney.

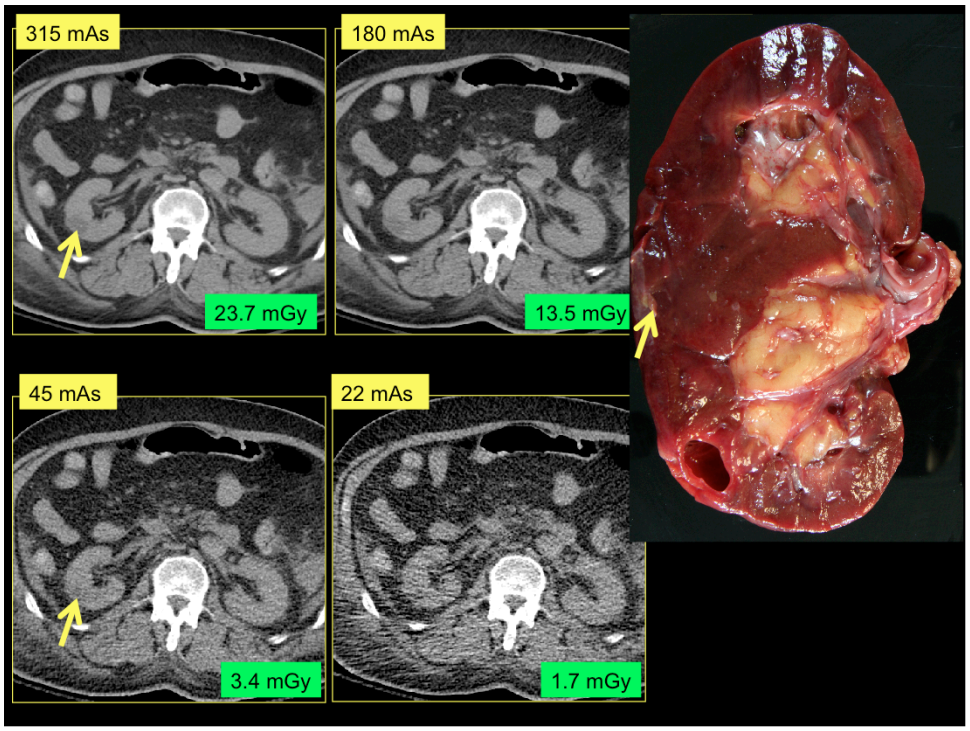

Figure 2b: Post mortem abdominal CT images of a 60 year old male (82 kg) at various tube currents. Image noise increases as the tube current is lowered and interferes with the visibility of right renal low attenuation lesion (arrow). His autopsy report confirmed presence of cysts in the mid and lower pole of the right kidney.

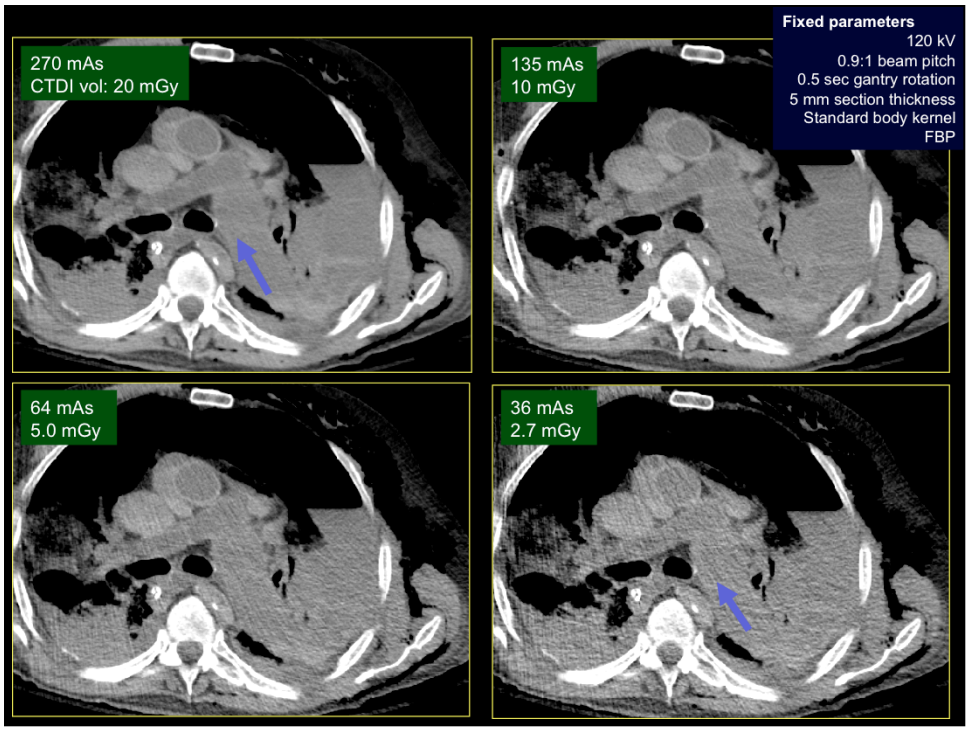

Figure 3a: Post mortem chest CT of a 70 year old male (72 kg) with known diagnosis of left pulmonary artery angiosarcoma at various tube currents. Low dose images acquired at 36 mAs (CTDIvol: 2.7 mGy) have higher image noise, however shows the enlarged left main pulmonary artery (arrows), subcutaneous emphysema and left hydropneumothorax. Acceptability of low dose images would have certainly improved with administration of intravenous contrast and lower kV.

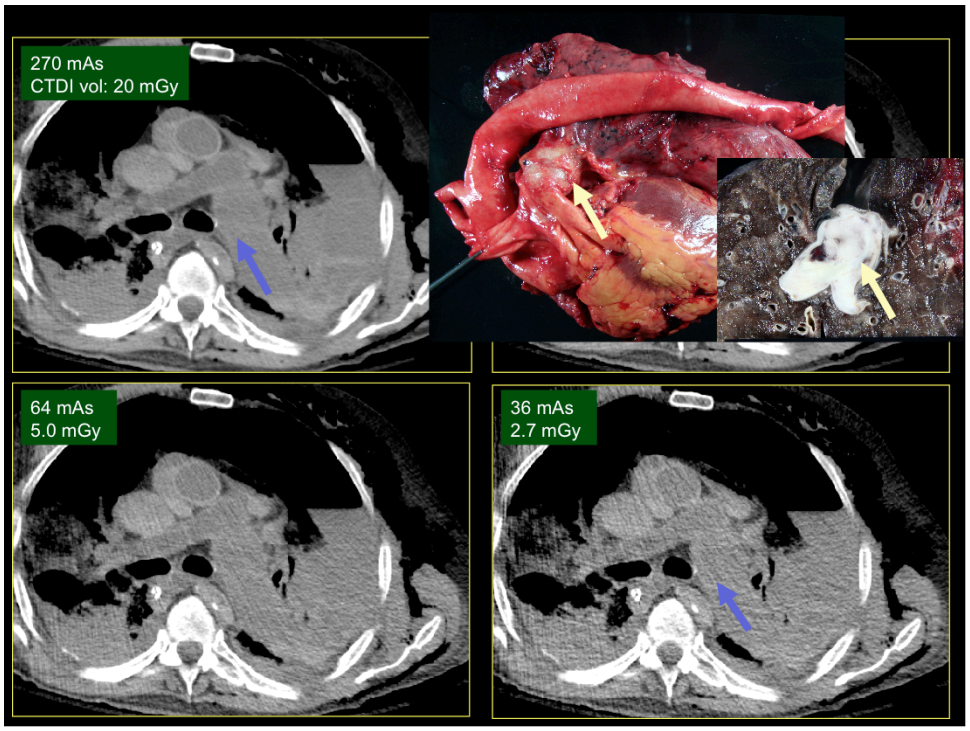

Figure 3b: Post mortem chest CT of a 70 year old male (72 kg) with known diagnosis of left pulmonary artery angiosarcoma at various tube currents. Low dose images acquired at 36 mAs (CTDIvol: 2.7 mGy) have higher image noise, however shows the enlarged left main pulmonary artery, right lower lobe atelectasis, subcutaneous emphysema and left hydropneumothorax. Acceptability of low dose images would have certainly improved with administration of intravenous contrast and lower kV.

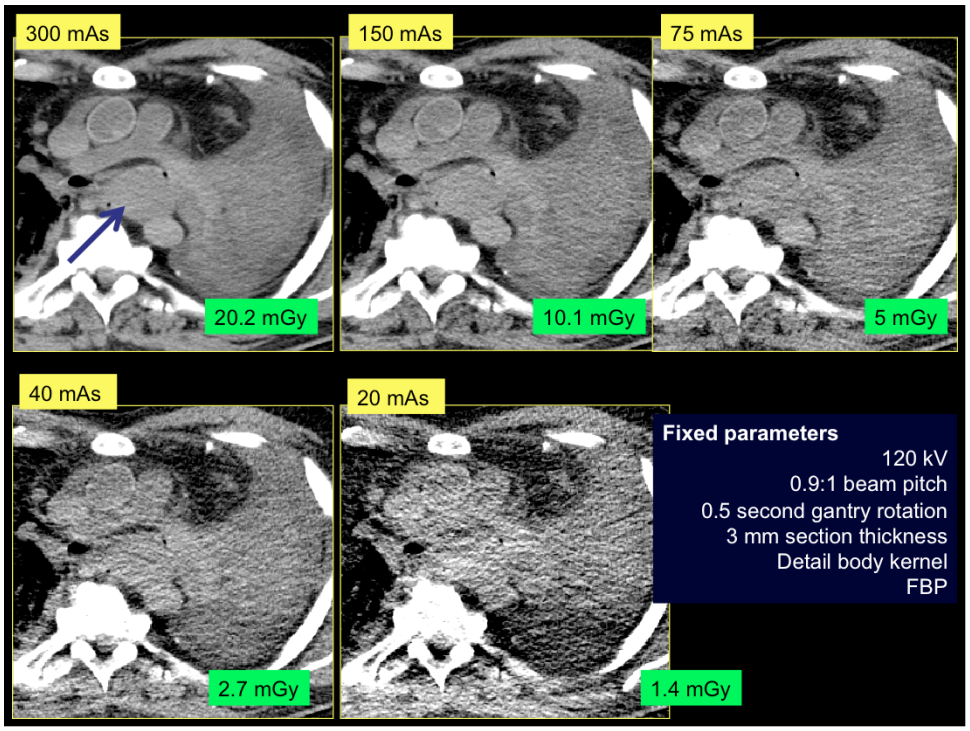

Figure 4a: A 70 year old male (89 kg) with post mortem chest CT at various tube currents. The 75 mAs (CTDIvol 5 mGy) image shows 6.5 * 4 cm mediastinal mass (arrow) located posterior to pulmonary artery bifurcation, superior left atrium and anterior to descending aorta, with additional findings of collapsed left lung and pleural effusion. Further reduction of tube current (40 and 20 mAs) results in increased image noise affecting the detection of edges of the mediastinal mass as well as left pleural effusion. The lesson here is that for mediastinal abnormalities higher dose is necessary as compared to primary lung abnormalities. Tailoring of CT protocols based on clinical indications is important. For screening protocols or primary lung pathologies much lower dose CT is sufficient, whereas in patients with advanced disease or mediastinal abnormalities, a higher dose may be necessary. Once again, addition of intravenous contrast would have improved the contrast to noise ratio of the mediastinal lesions at lower dose images.

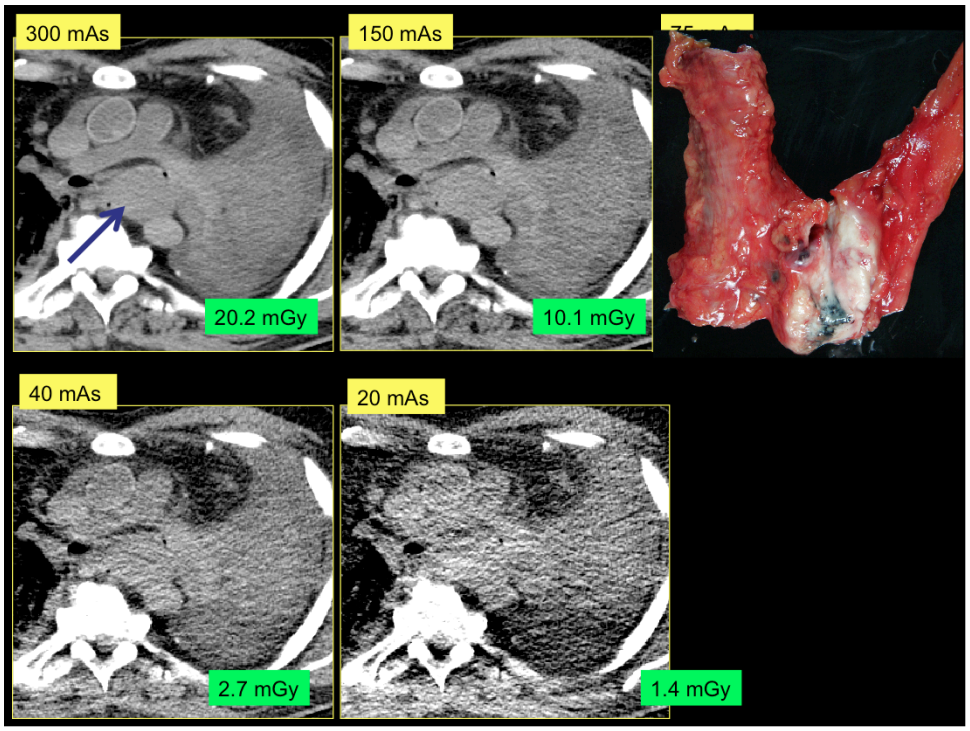

Figure 4b: A 70 year old male (89 kg) with post mortem chest CT at various tube currents. The 75 mAs (CTDIvol 5 mGy) image shows 6.5 * 4 cm mediastinal mass (arrow) located posterior to pulmonary artery bifurcation, superior left atrium and anterior to descending aorta, with additional findings of collapsed left lung and pleural effusion. Further reduction of tube current (40 and 20 mAs) results in increased image noise affecting the detection of edges of the mediastinal mass as well as left pleural effusion. The lesson here is that for mediastinal abnormalities higher dose is necessary as compared to primary lung abnormalities. Tailoring of CT protocols based on clinical indications is important. For screening protocols or primary lung pathologies much lower dose CT is sufficient, whereas in patients with advanced disease or mediastinal abnormalities, a higher dose may be necessary. Once again, addition of intravenous contrast would have improved the contrast to noise ratio of the mediastinal lesions at lower dose images.

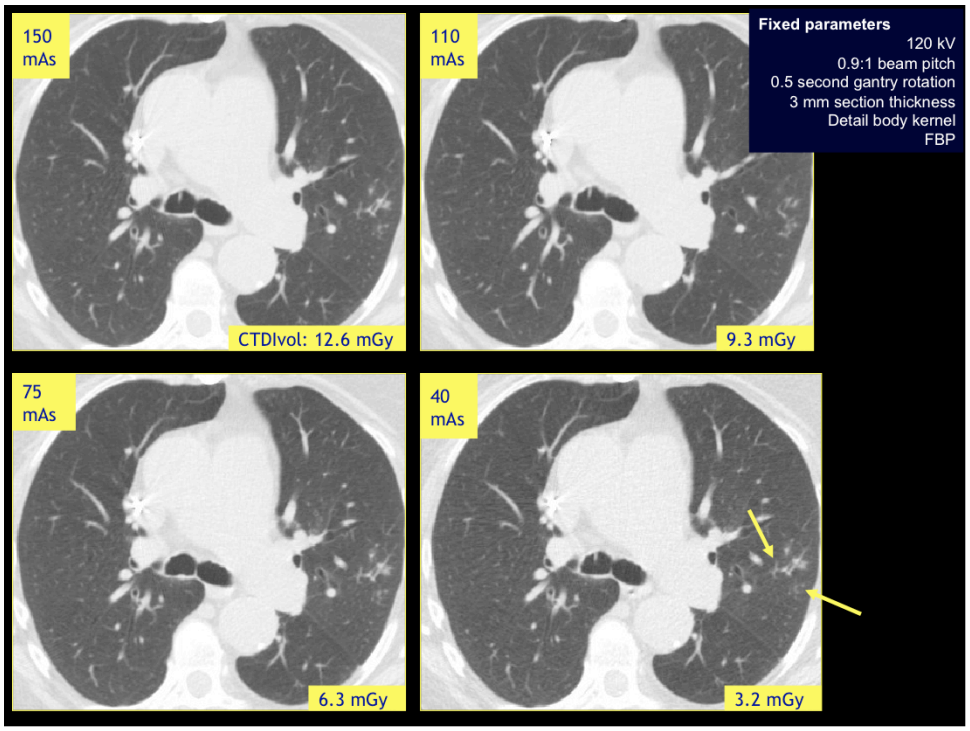

Figure 5: Chest CT acquired at various tube currents with a limited scan length of 10 cm to limit the total radiation exposure to the patient. Increased image noise noted in mediastinum is barely apparent in the lungs due to high background contrast between air and soft tissue density lung lesions and vessels. Note that four fold reduction in dose from 150 mAs to 40 mAs (3.2 mGy), has hardly any affect on visibility of small structures, left major fissure and clustered nodular opacity (arrow) in the left upper lobe.

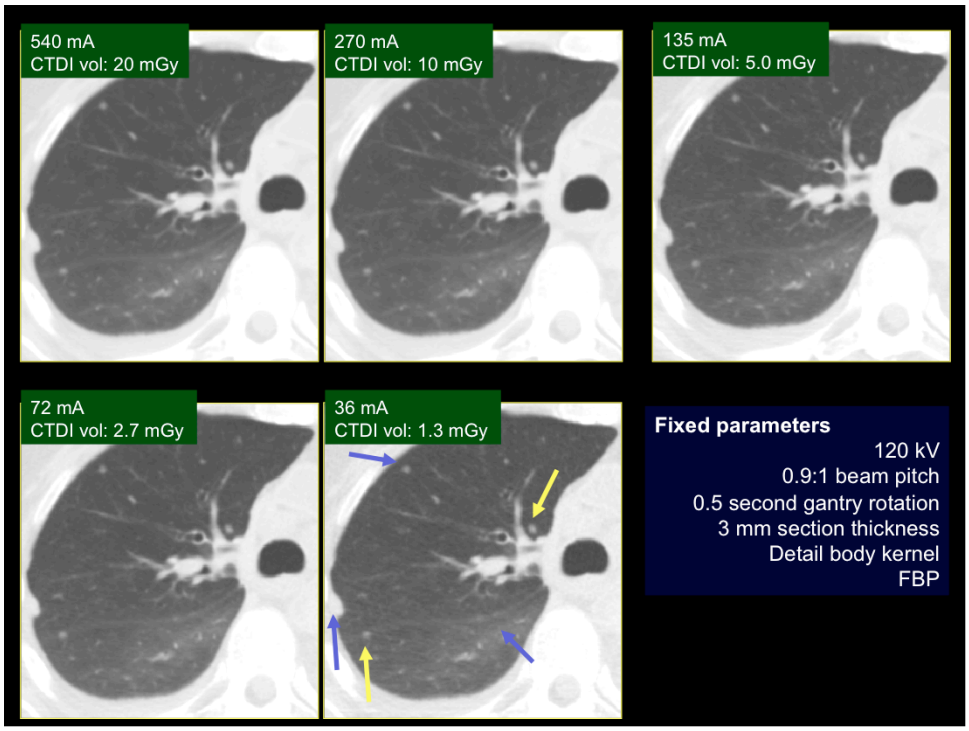

Figure 6a: Post mortem chest CT of a 60 year old female (52 kg) with known diagnosis of metastatic papillary carcinoma at various tube current levels. Low radiation dose image (18 mAs, CTDIvol: 1.3 mGy) show right pleural and pulmonary nodules as well as ground glass opacities (arrows) in right lower lobe.

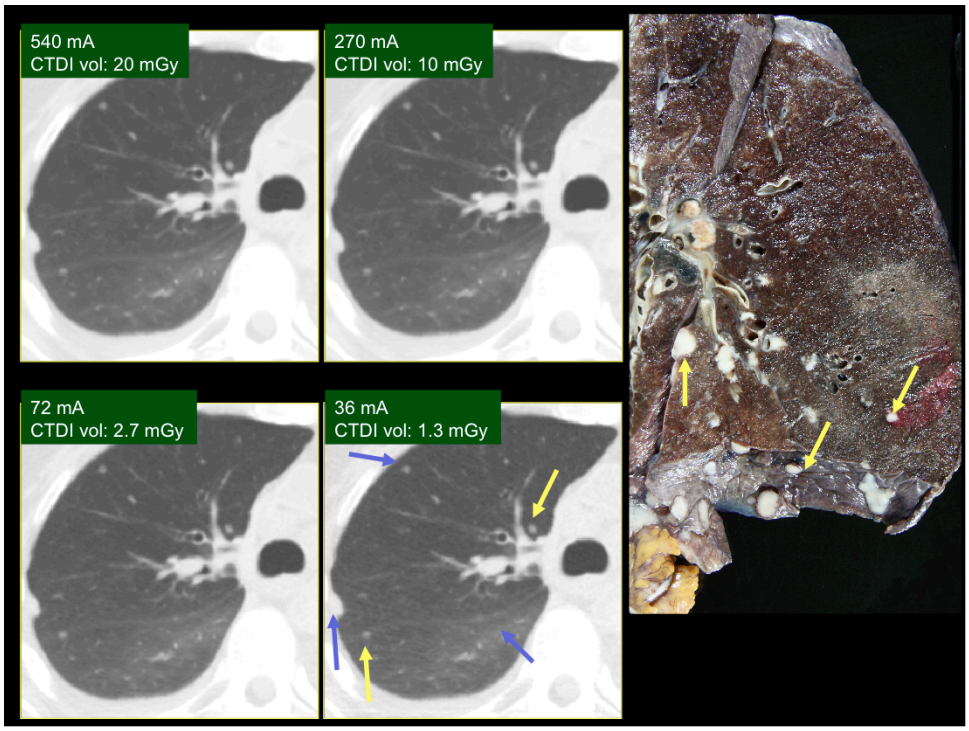

Figure 6b: Post mortem chest CT of a 60 year old female (52 kg) with known diagnosis of metastatic papillary carcinoma at various tube current levels. Low radiation dose image (18 mAs, CTDIvol: 1.3 mGy) show right pleural and pulmonary nodules as well as ground glass opacities (arrows) in right lower lobe.

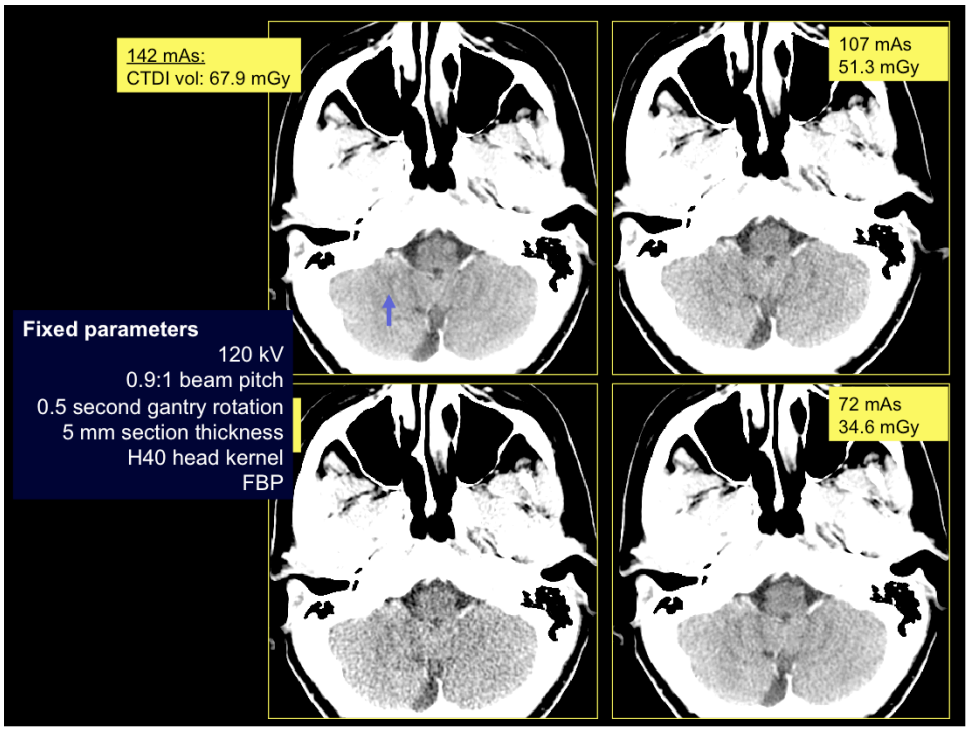

Figure 7: Head CT acquired at various tube currents with a limited scan length of 10 cm to limit the total radiation exposure. increased image noise in low dose image at 35 mAs (16.7 mGy) limits the visibility of grey white matter (arrow) in the cerebellum surrounded by thick cranial bones.

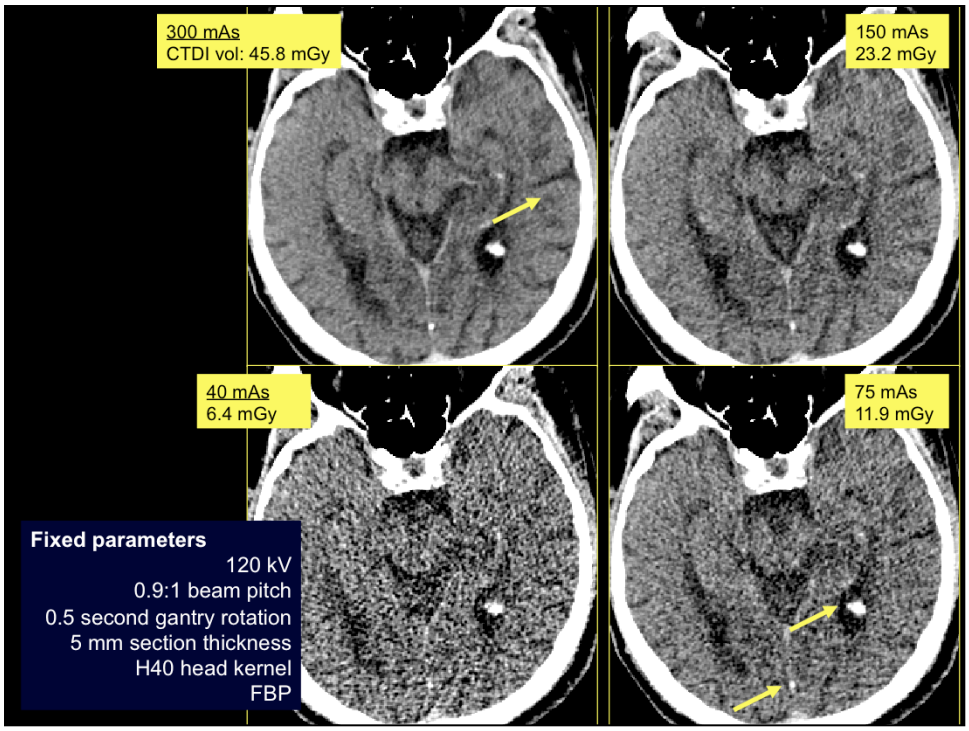

Figure 8: Post mortem head CT acquired at various tube currents shows increased image noise in low dose images, which affects the delineation of low contrast structures, such as, sulci and gyri (arrow) while retaining the visibility or detection of high contrast small structures, such as choroid plexus (arrow) and calcified spec in the posterior falx (arrow).

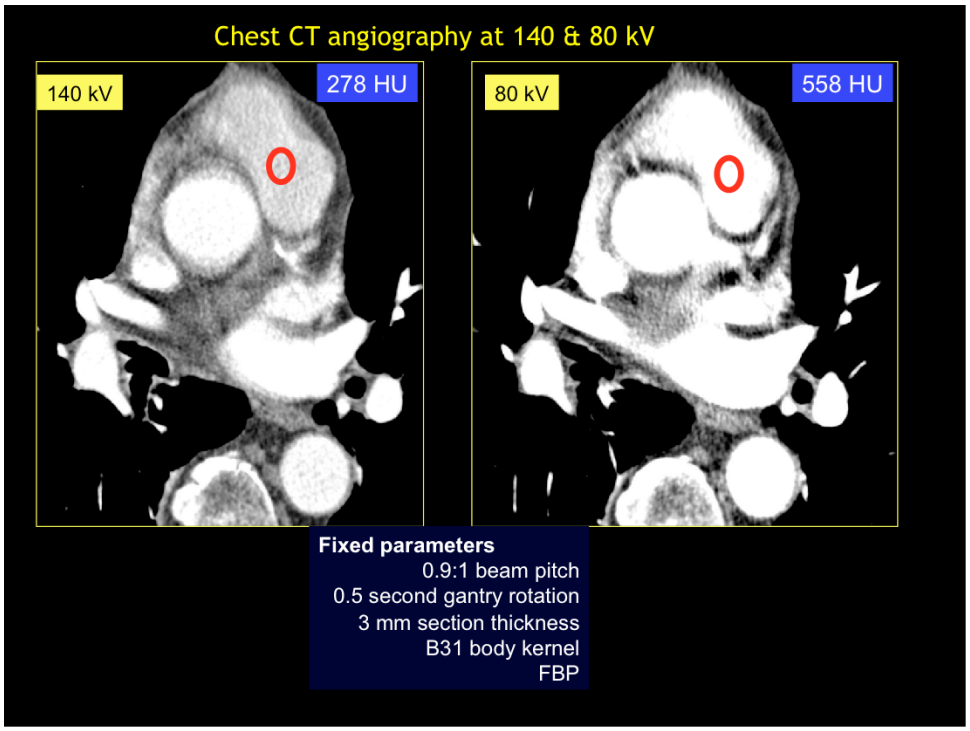

Figure 9: Chest CT angiography performed at varying 140 and 80 kV. Lowered kV (80 kV) shows incre

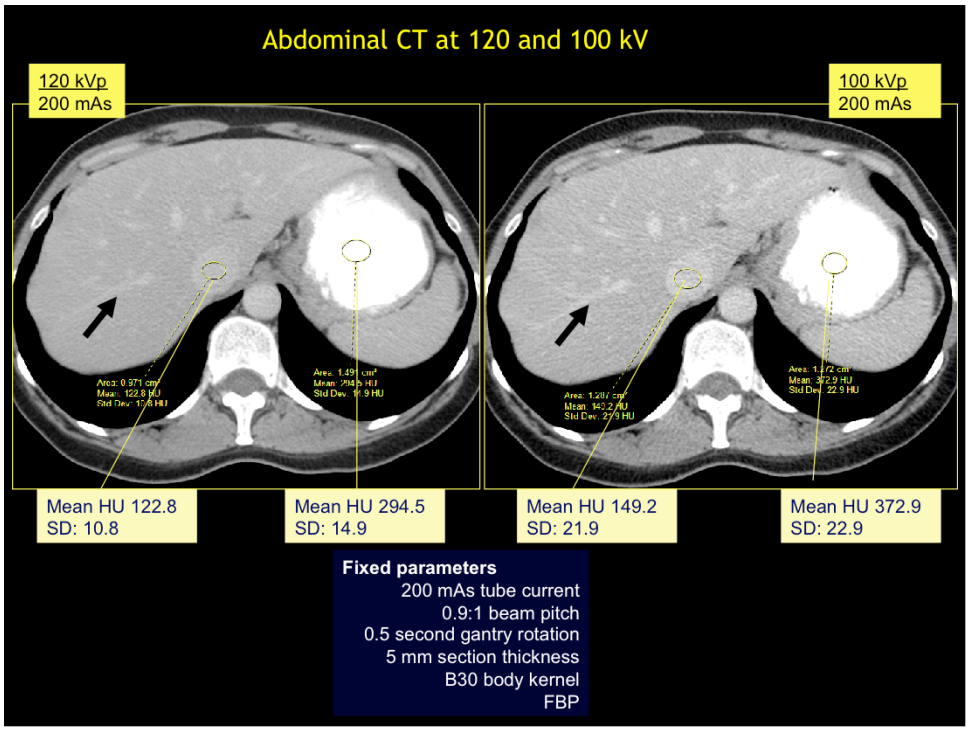

Figure 10: Contrast enhanced abdominal CT performed at varying kV of 120 and 100. Lower kV results in increased image noise in hepatic parenchyma but also allows better visibility of hepatic vessels. For arterial phase imaging of the abdominal structures, low kV (80-100kV) should be applied in at least small to medium size patients in order to improve the image contrast and reduce radiation dose. In larger patients, 120 kV may be more suitable for abdominal imaging in arterial phase.

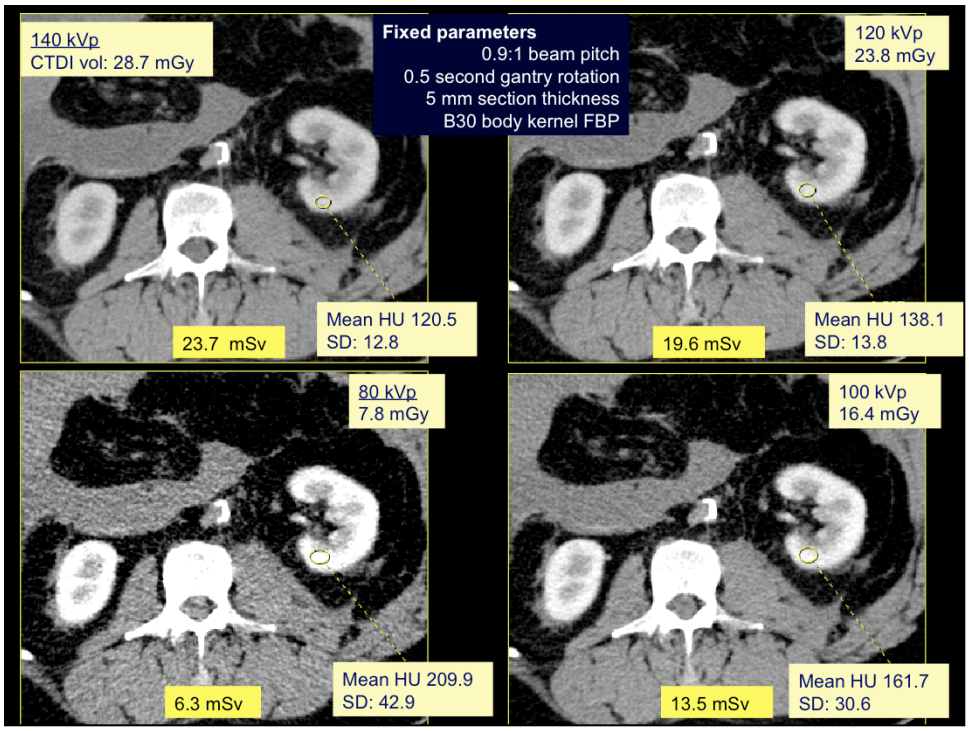

Figure 11: Post mortem CT at different kV settings in a patient with renal failure shows retained contrast and persistent nephrogram from pre-mortem CT. Lower kV results in increased image noise in soft tissue and paravertebral muscles, but also increases the CT numbers of contrast enhanced renal parenchyma. Objective measurements by placing region of interests in left renal cortex show increased image noise and increased HU values at lower kV images.

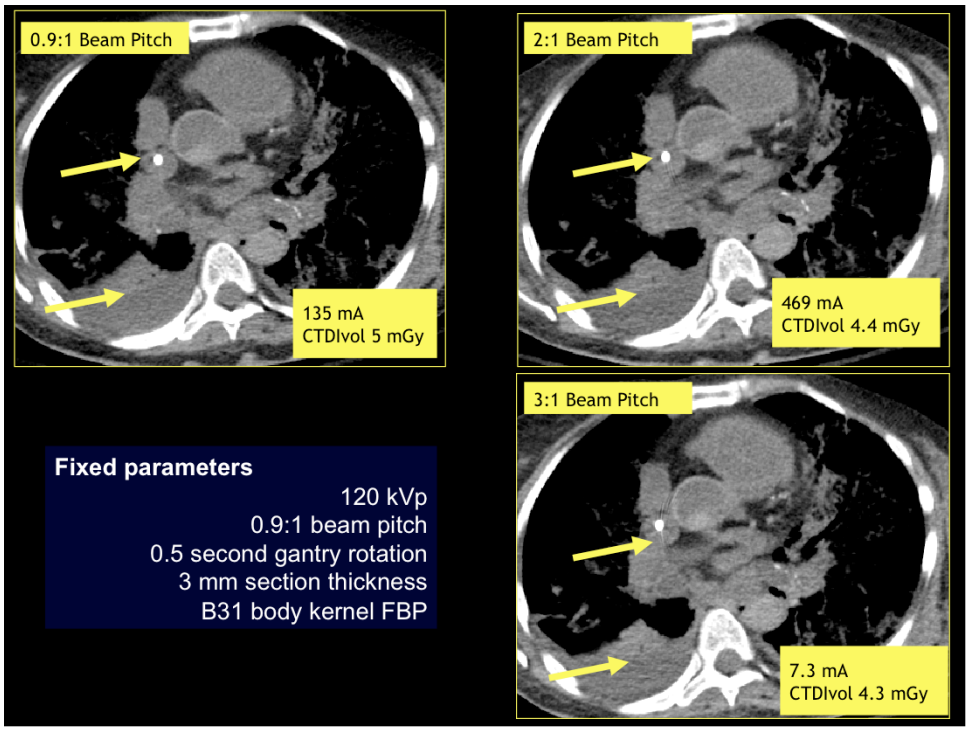

Figure 12: Postmortem chest CT at different beam pitches in a 60 year old female (54 kg) with known diagnosis of uterine adenocarcinoma. Transverse chest CT images acquired at higher beam pitch results in higher image noise in the mediastinum and helical artifacts due to high catheter in SVC (arrow).

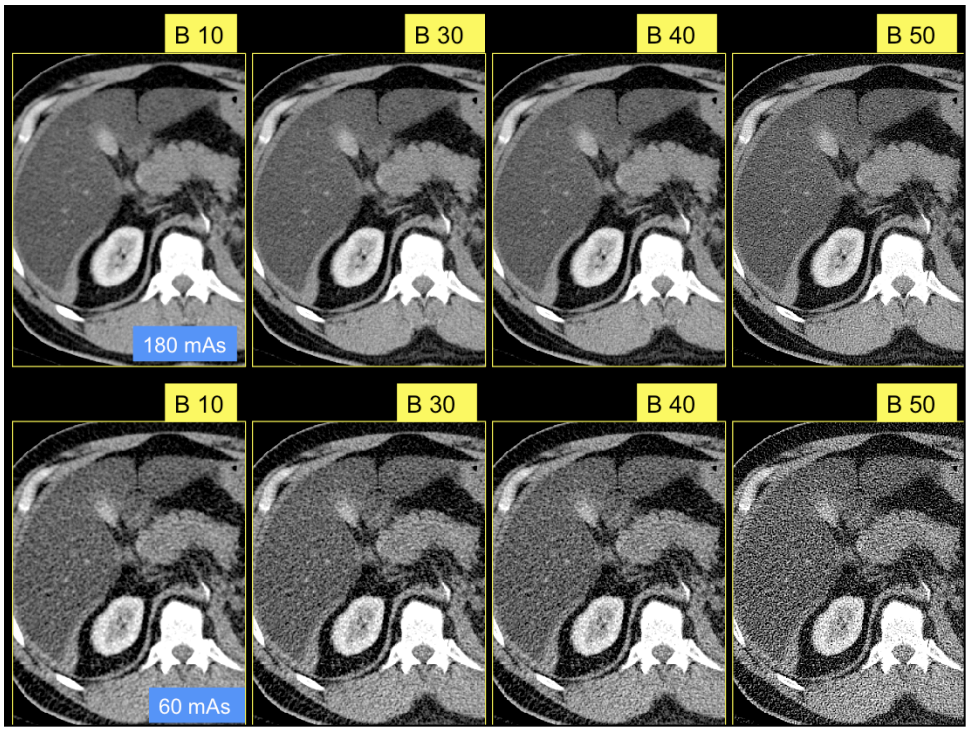

Figure 13: Image reconstruction kernels plays an important role in balancing image noise and sharpness

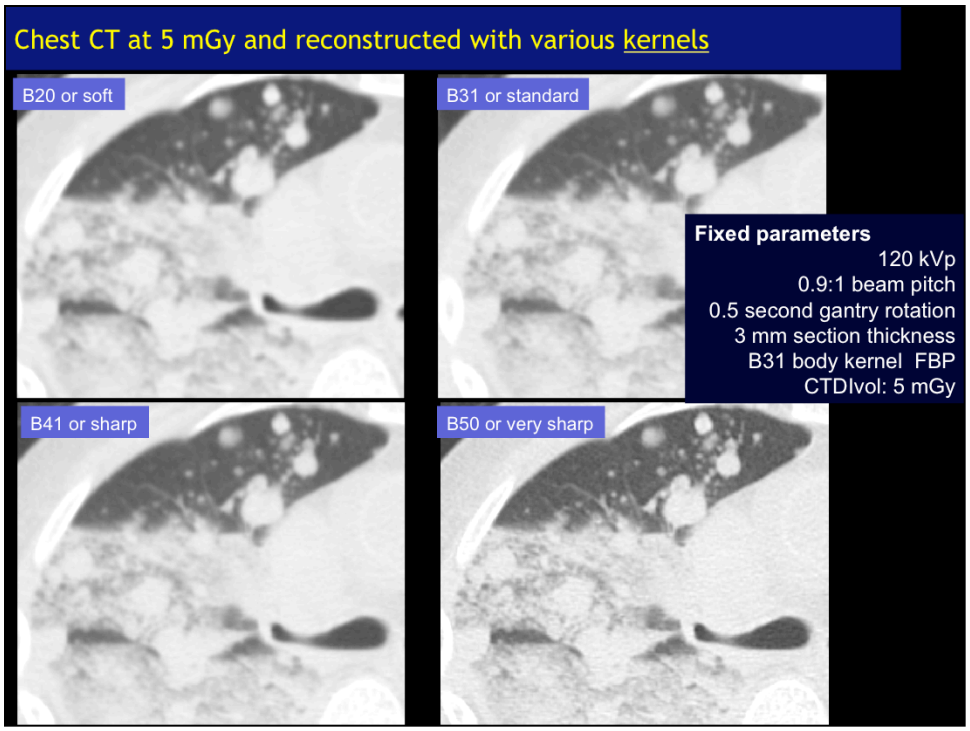

Figure 14: Transverse chest CT images acquired at 75 mAs (CTDIvol 5 mGy) and reconstructed with va

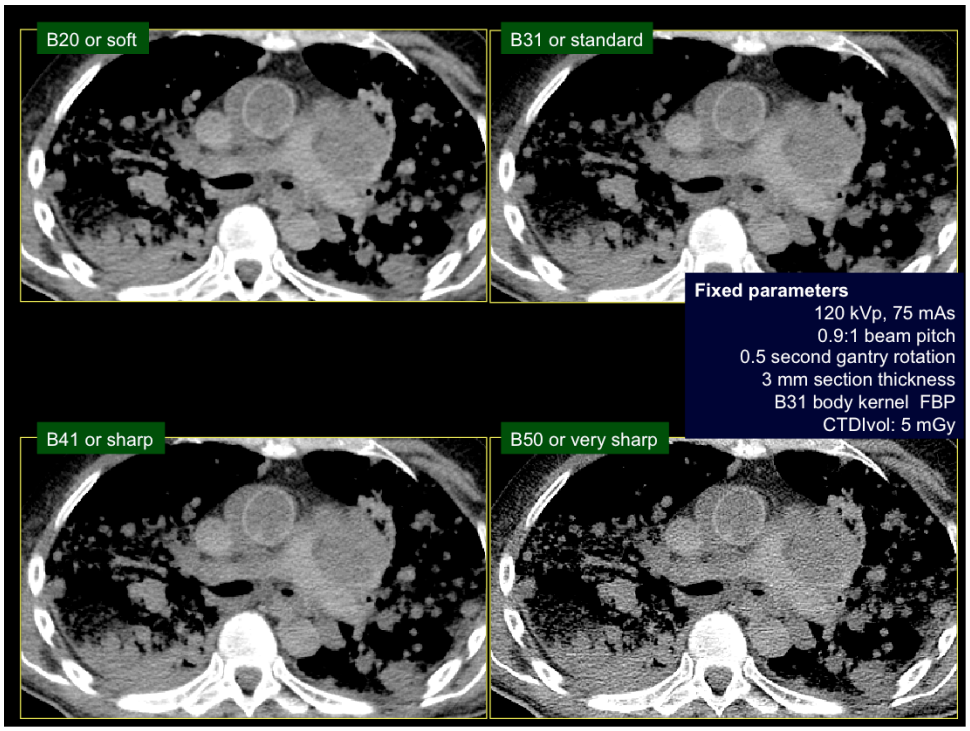

Figure 15: Transverse chest CT images in mediastinal windows at various kernels (B20 to B50). B20 im

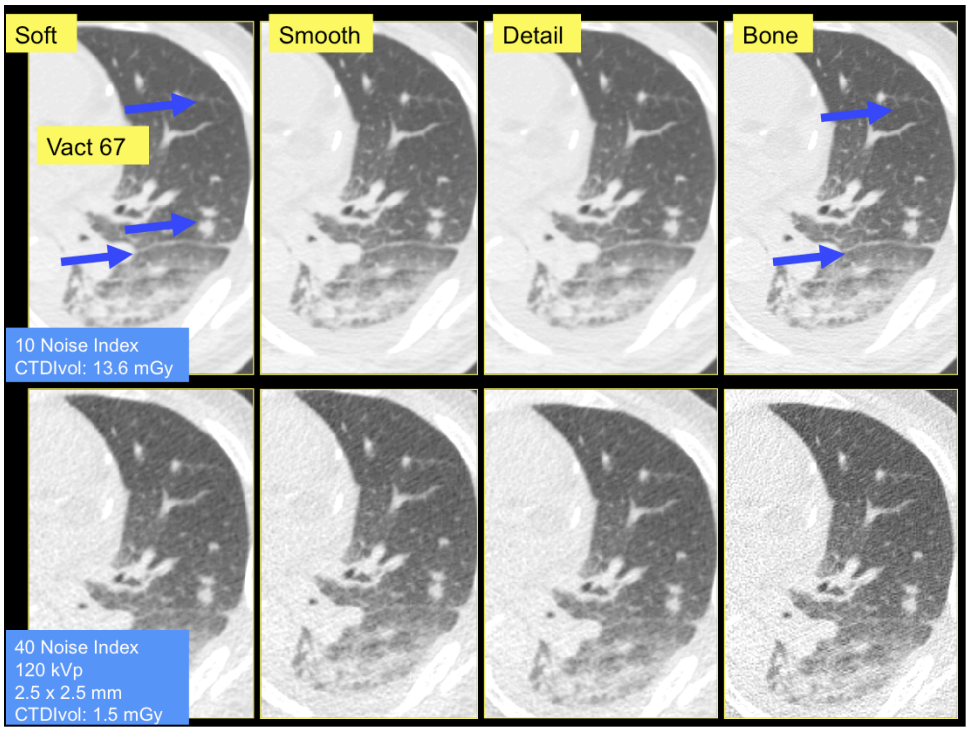

Figure 16: Transverse chest CT images acquired at two dose levels (higher dose: 10 noise index (upper

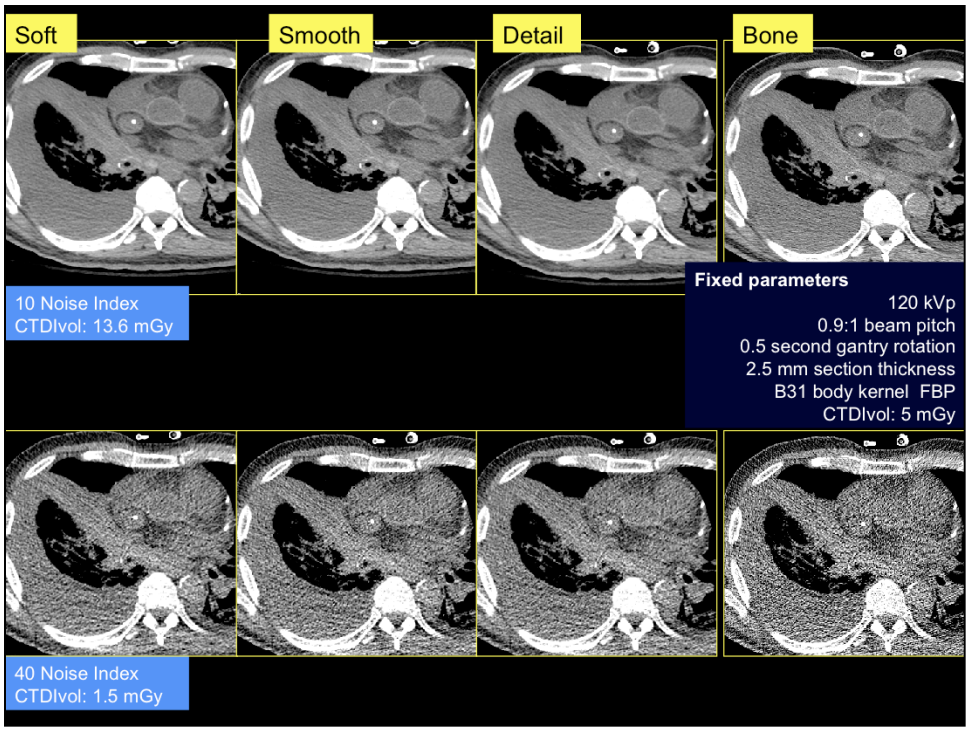

Figure 17: Transverse chest CT images in mediastinal windows acquired at two dose levels (higher dose

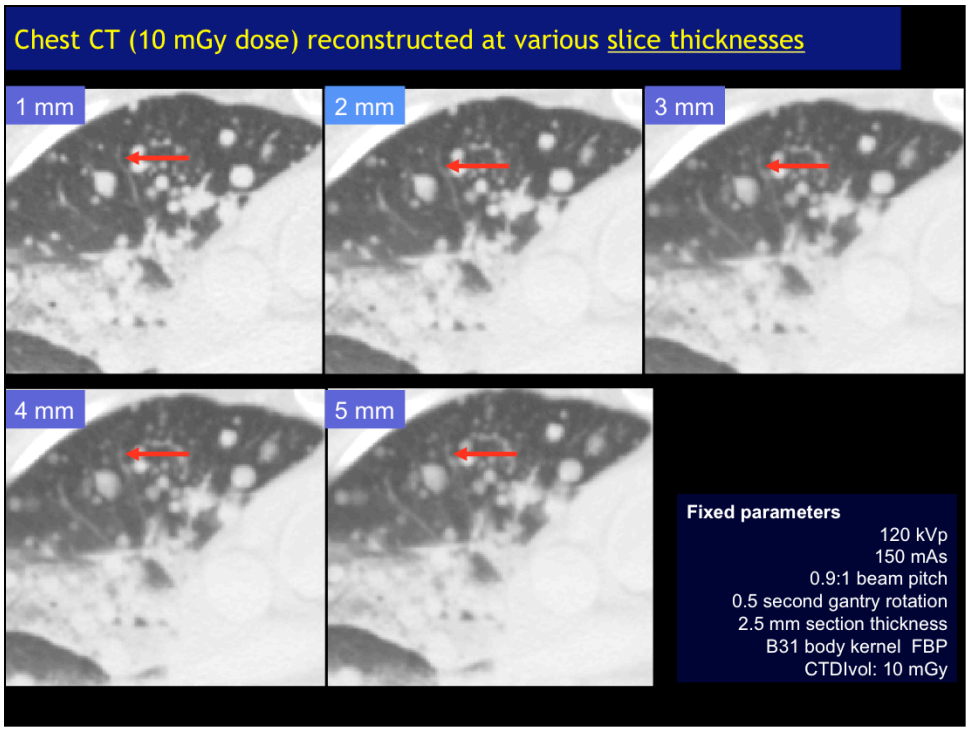

Figure 18: Transverse chest CT images acquired at 150 mAs (CTDIvol 10 mGy) and reconstructed at di

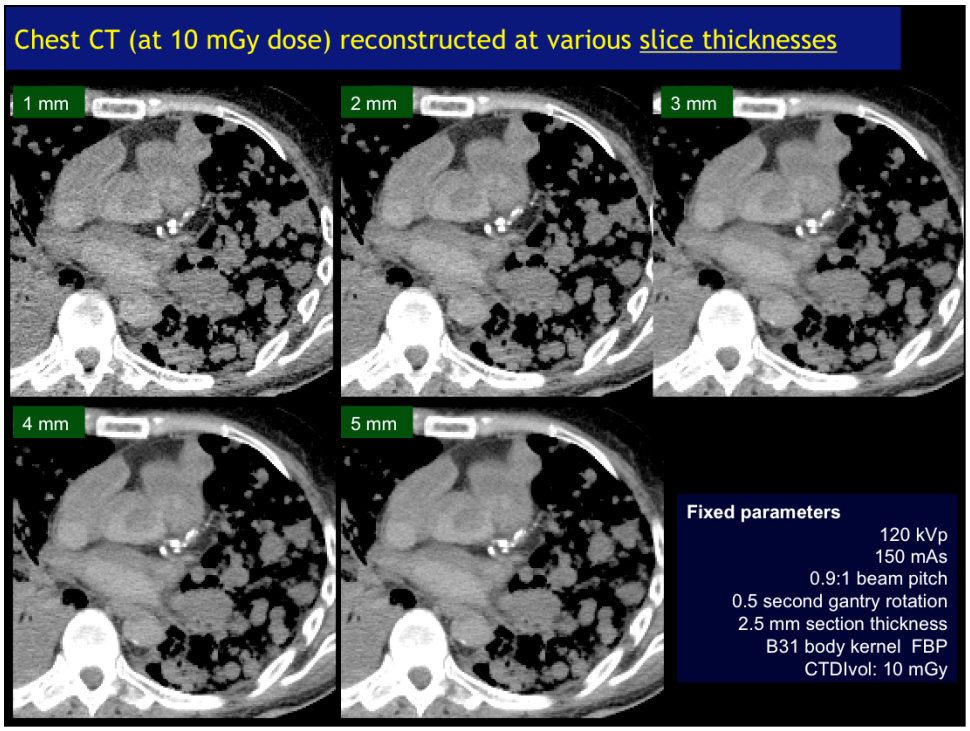

Figure 19: Transverse chest CT images (mediastinal windows) acquired at 150 mAs (CTDIvol 10 mGy)

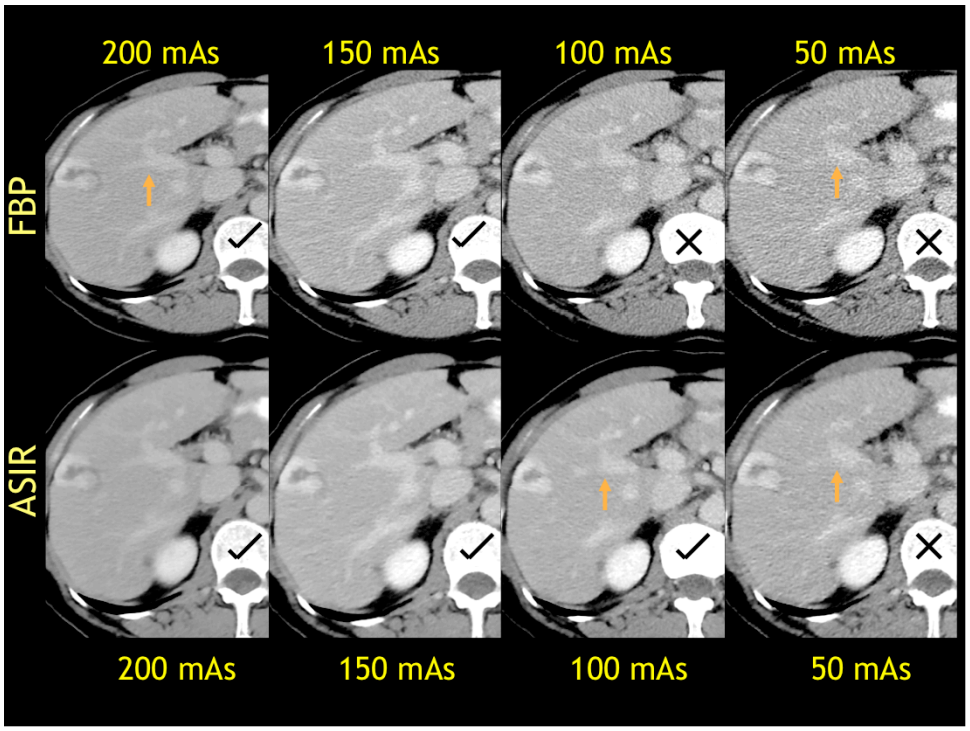

Figure 20: Transverse abdominal CT images in a 51 year old woman (63 kg) with a right hepatic lobe enhancing lesion (hemangioma) in segment 5 was acquired at four tube current levels (200, 150, 100 and 50 mAs) and resultant radiation dose levels (16.4, 12.6, 8.4 and 4.2 mGy) were reconstructed with FBP and iterative reconstruction technique (Adaptive Statistical Iterative Reconstruction, ASIR, GE Healthcare). ASIR enabled images shows lower image noise at each dose levels. However, compared to other dose levels at 4.2 mGy, visibility of the hepatic veins is compromised in both FBP and ASIR images.

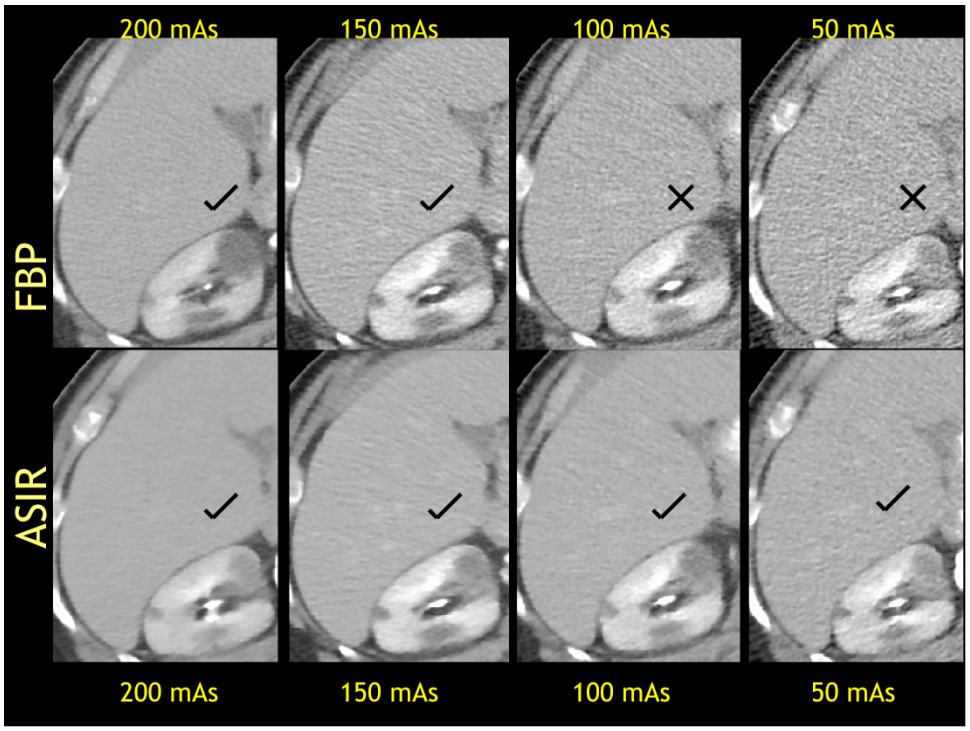

Figure 21: Transverse abdominal CT images acquired at four tube current levels (200, 150, 100 and 50 mAs) and resultant radiation dose levels (16.4, 12.6, 8.4 and 4.2 mGy) were reconstructed with FBP and iterative reconstruction technique (Adaptive Statistical Iterative Reconstruction, ASIR, GE Healthcare). ASIR enabled images shows lower image noise at each dose level and better visibility of low attenuating renal lesions.

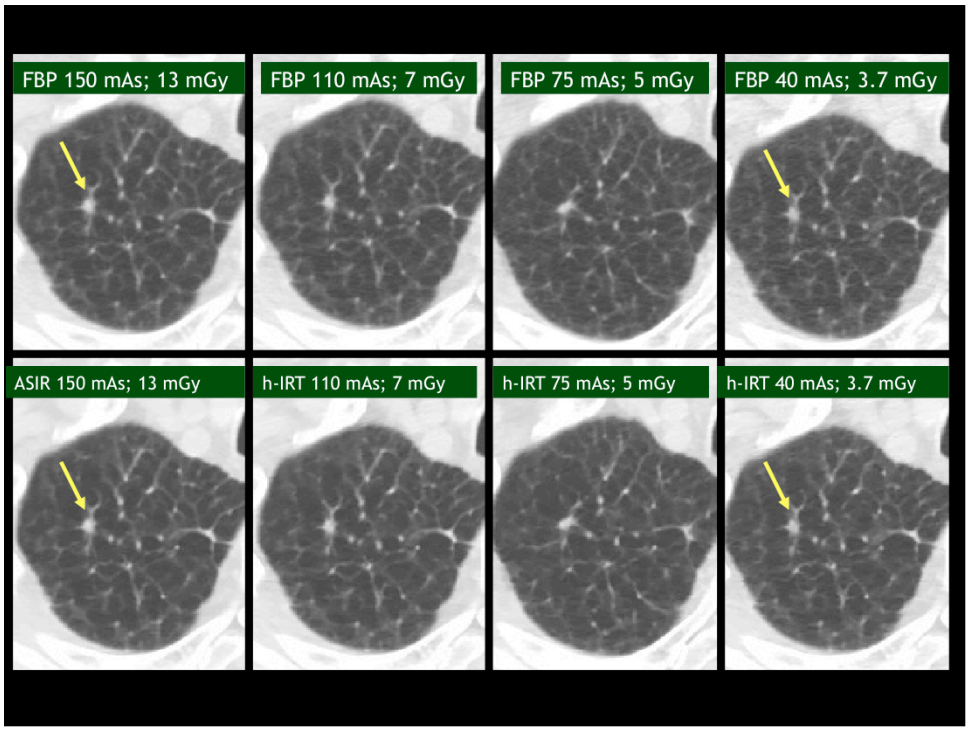

Figure 22: Transverse chest CT images acquired at four tube current levels (150, 110, 75 and 40 mAs) were reconstructed with FBP and iterative reconstruction technique (Adaptive Statistical Iterative Reconstruction, ASIR, GE Healthcare). Both ASIR and FBP images show right upper lobe pulmonary nodule. Although ASIR enabled images shows lower image noise, the visibility of lesions is equal on low dose FBP and ASIR images.

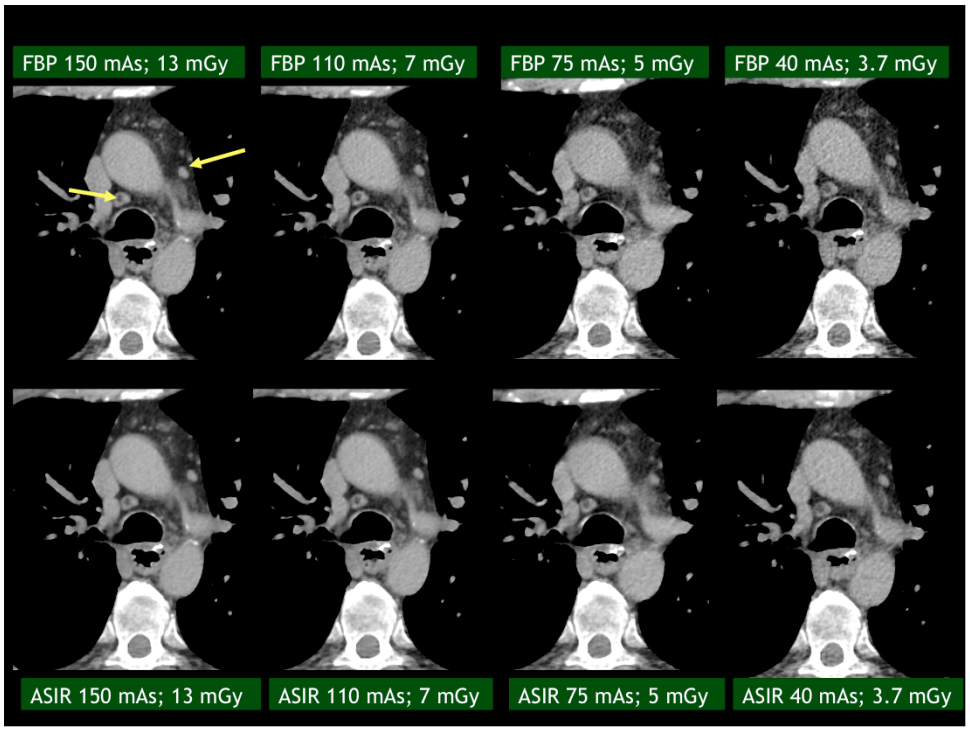

Figure 23: Transverse chest CT images (mediastinal windows) acquired at four tube current levels (150, 110, 75 and 40 mAs) were reconstructed with FBP and iterative reconstruction technique (Adaptive Statistical Iterative Reconstruction, ASIR, GE Healthcare). Both ASIR and FBP shows right paratracheal and mediastinal lymph nodes, however ASIR enabled images have lower image noise and better visibility of lymph nodes at lower tube current of 40 mAs.

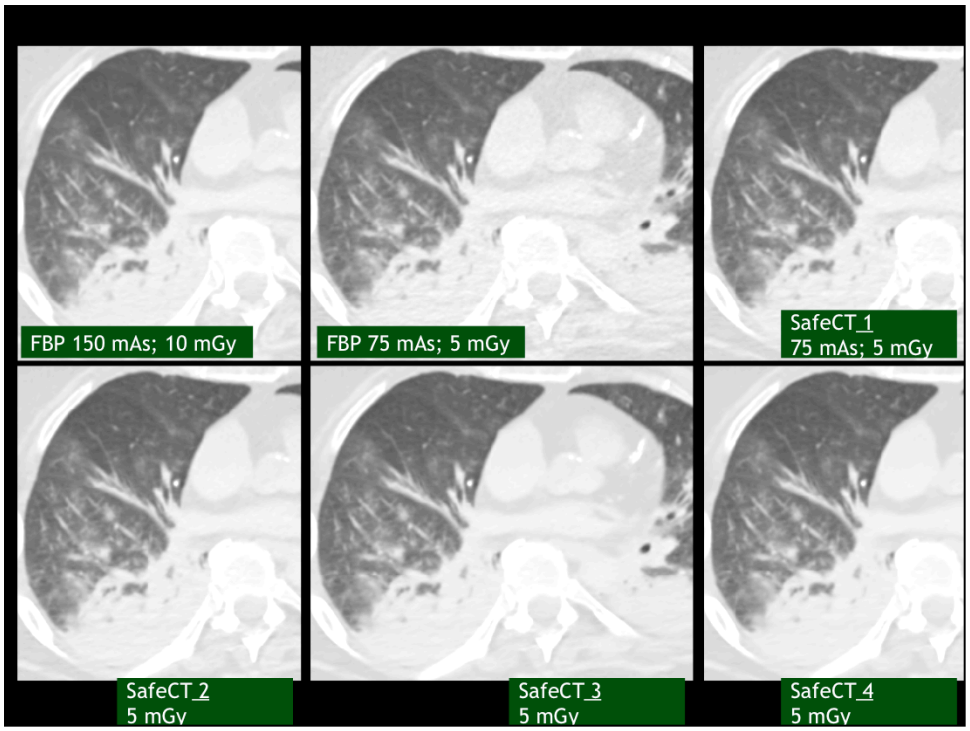

Figure 24: Transverse chest CT images demonstrate pneumonia and/or atelectasis in right lower lobe. L

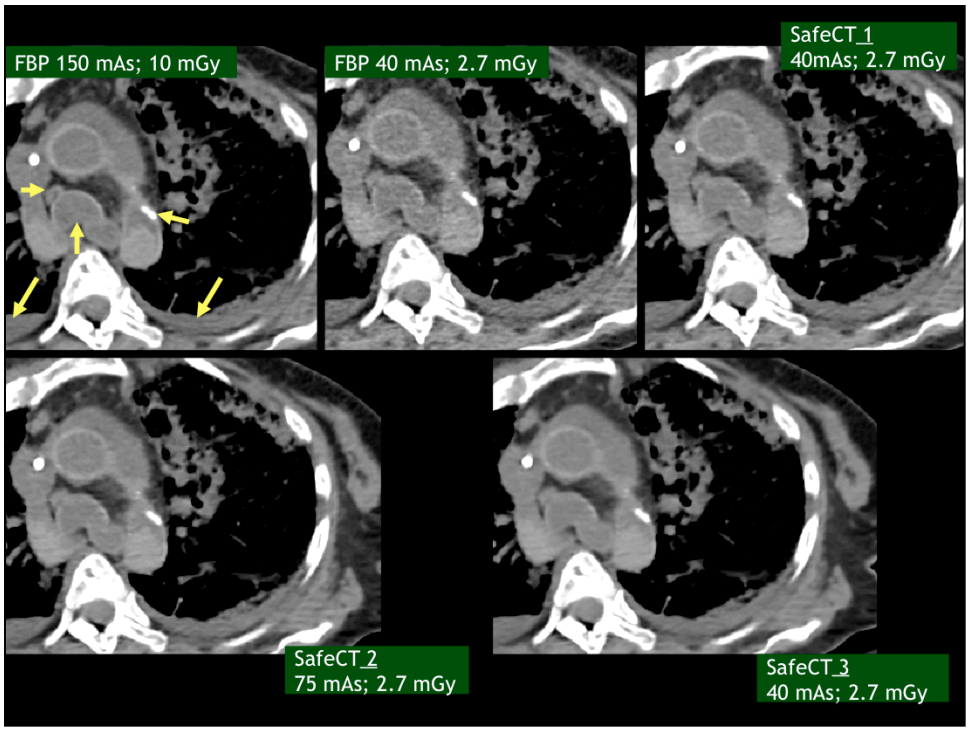

Figure 25: Transverse chest CT images (mediastinal windows) showing paratracheal lymph node, fluid

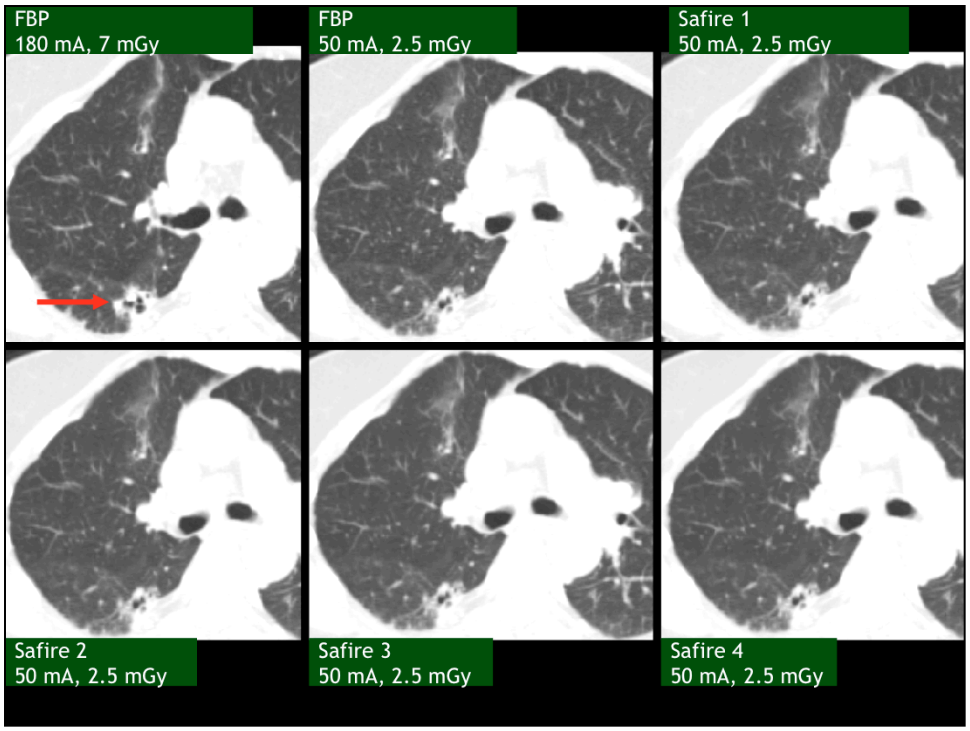

Figure 26: Transverse chest CT images showing solid and cystic opacity in the right lower lobe with bro

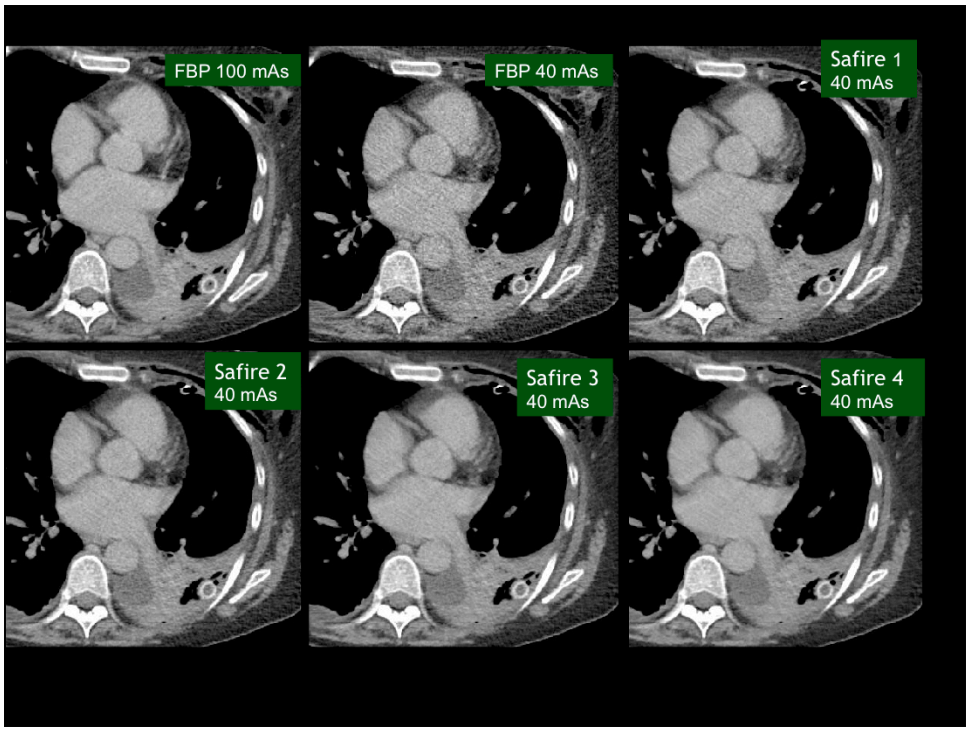

Figure 27: Transverse chest CT images showing loculated left pleural effusion, left lower lobe pneumonia and/or atelectasis, acquired at two tube current levels (100 mAs or 7 mGy & 40 mAs or 2.5 mGy). Low dose images (40 mAs) were reconstructed with iterative reconstruction techniques (Sinogram Affirmed Iterative Reconstruction, SAFIRE, Siemens Healthcare) at various settings (settings 1-4). Higher settings of the reconstruction technique results in lower image noise and allowing reduction of tube current.

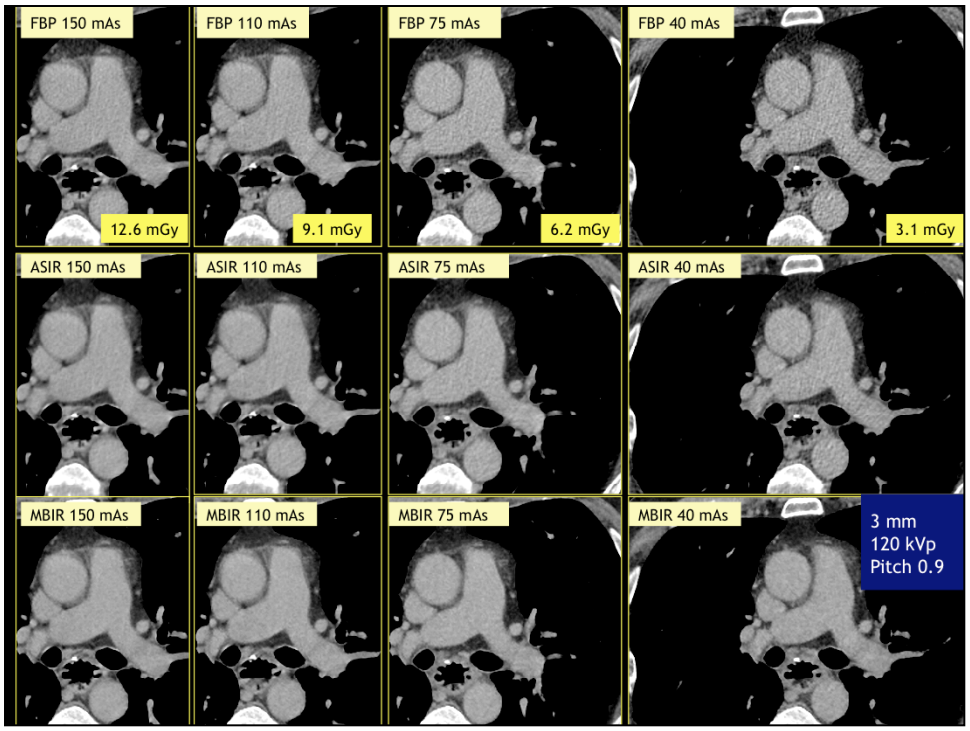

Figure 28: Transverse chest CT images (mediastinal windows) acquired at four tube current levels (150, 110, 75 and 40 mAs) were reconstructed with FBP (top row) and two iterative reconstruction techniques [Adaptive Statistical Iterative Reconstruction, ASIR (middle row) and Model Based Iterative Reconstruction, MBIR, GE Healthcare (bottom row)]. Both ASIR and MBIR enabled images show lower image noise at all dose levels, except at the lowest radiation dose (3.1 mGy), ASIR technique has lower image noise compared to FBP, whereas MBIR image has the lowest image noise (even when compared to the 150 mAs FBP image).

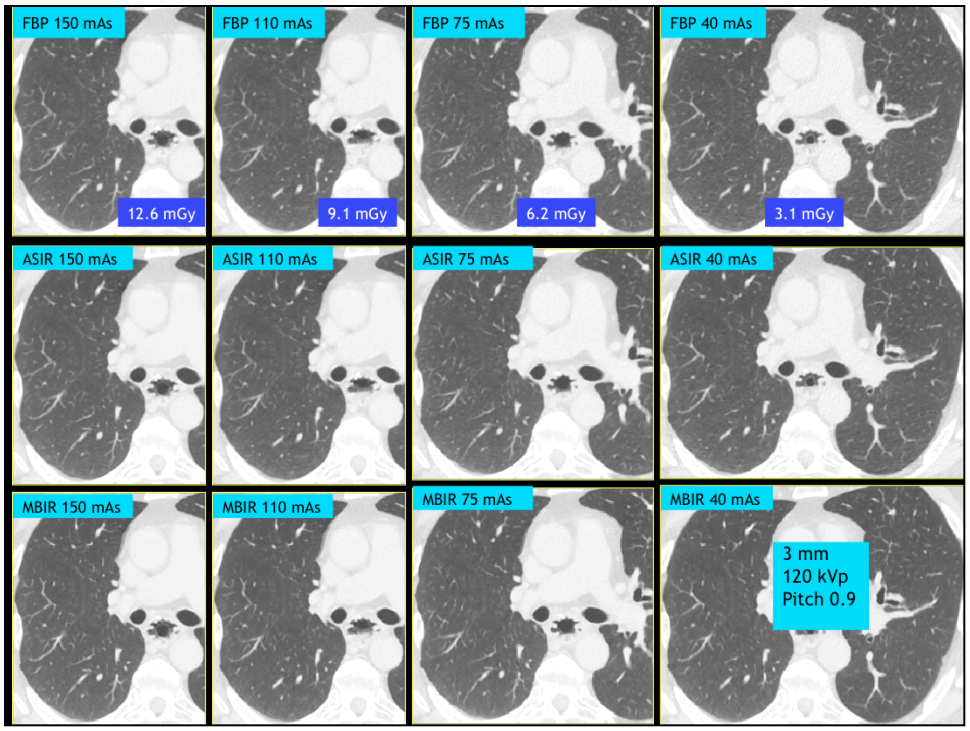

Figure 29: Transverse chest CT images acquired at four tube current levels (150, 110, 75 and 40 mAs) were reconstructed with FBP (top row) and iterative reconstruction technique [Adaptive Statistical Iterative Reconstruction, ASIR (middle row) and Model Based Iterative Reconstruction, MBIR (bottom row)]. Although ASIR and MBIR reconstructed images have lower image noise compared to corresponding FBP images, at these dose levels there is no difference in visualization of lung parenchyma between the three techniques.

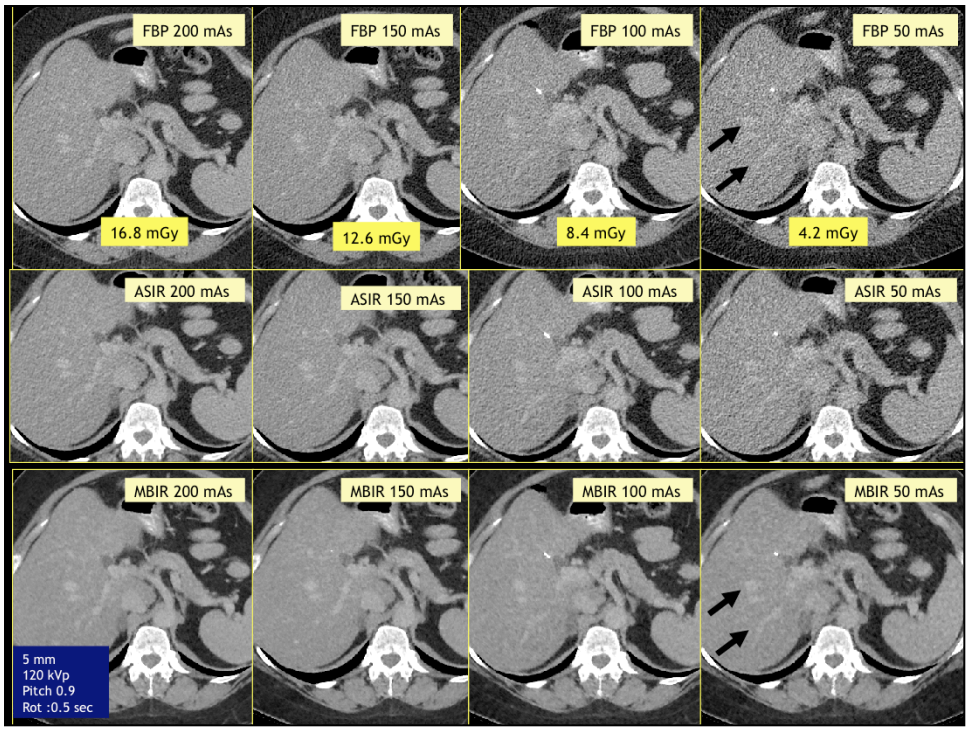

Figure 30: Transverse abdominal CT images acquired at four tube current levels (200, 150, 100 and 50 mAs) were reconstructed with FBP (top row) and iterative reconstruction technique [Adaptive Statistical Iterative Reconstruction, ASIR (middle row) and Model Based Iterative Reconstruction, MBIR (bottom row)]. Both ASIR and MBIR images have lower image noise at all dose levels, except at lowest radiation dose (50 mAs, CTDIvol 4.2 mGy), where ASIR image was deemed unacceptable for noise while MBIR lowers the image noise in the hepatic parenchyma and enhances the visibility of hepatic vessels (arrows).

Thank You

Please contact for any questions

Sarabjeet Singh, MD: ssingh6@partners.org

Mannudeep K Kalra, MD: mkalra@partners.org